Practical characterization and modeling method for macroscopic gas–solid flow in circulating fluidized bed

Ritvanen Jouni, Chechurin Yegor, Hyppänen Timo

DOI: 10.1016/j.cej.2020.127819

Practical characterization and modeling method for macroscopic gas–solid flow in circulating fluidized bed

Jouni Ritvanen*, Yegor Chechurin, Timo Hyppänen

Lappeenranta-Lahti University of Technology, LUT School of Energy Systems, P.O. Box 20, FI-53851 Lappeenranta, Finland

Abstract

Fluidized beds are common in the energy and chemical industries because they provide a good environment for heterogeneous reactions owing to the combination of mixing and multiphase flow hydrodynamics. The hydrodynamics of gas–solid suspensions in fluidized beds is extremely complicated and requires accurate study. A wide range of simulation approaches have been used in fluidized bed design and operational studies, but it is still not clear how the phase interaction should be treated. In this study, a practical characterization method and modeling tool for gas–solid flows are presented, along with a definition of the phase interaction. In this method, the phase interaction is derived for a real solid material with specific particle size, shape and density distributions. In addition, a macroscopic 1D modeling tool for

*Corresponding author

Email address: jouni.ritvanen@lut.fi (Jouni Ritvanen)

[1]DOI for final accepted article: 10.1016/j.cej.2020.127819

gas–solid flow that is capable of practical stationary and transient simulations is presented. This tool solves the governing equation for the solid-phase momentum and provides physical predictions for transient gas–solid flow investigations. The proposed characterization method and modeling tool are validated against experimental data.
Keywords: Gas–solid flow, drag correction, characterization, transient simulation

1. Introduction

Fluidized bed processes are widely used in energy technology and chemical processes. They have also been applied to solid looping technologies in carbon capture and storage. In these technologies, multiple fluidized bed reactors are interconnected so that solid material can be transported between them. Reactor coupling increases the system complexity, and the design of these processes is complicated. Fluidized beds provide a good environment for heterogeneous reactions owing to the combination of mixing and multiphase flow hydrodynamics. The efficient design and operation of fluidized beds requires good knowledge of the hydrodynamics under steady-state and transient conditions. Furthermore, the hydrodynamics of gas–solid suspensions in fluidized beds is an extremely complicated phenomenon to model, as

thoroughly described in the review by Wang [1].

A wide variety of simulation approaches have been used in fluidized bed design and operational studies. Conventional methods include the Eulerian–Eulerian and Eulerian–Lagrangian approaches to gas–solid flow modeling [2–6]. In these approaches, several simplifications and averaging procedures are applied. Averaged material properties and space-averaged governing equations are typically used, and in steady-state investigations, the governing equations are time-averaged. When particles are approximated as spheres and an average particle size is used, the effects of the particle size and shape distributions are lost. Note that solid transport and momentum exchange from the gas phase to the solid phase is proportional to the pressure field around individual particles caused by the gas flow. Some Eulerian–Lagrangian approaches include the option of using a particle size distribution. However, true consideration of the particle shape in the models is more complicated and rare. Using space-averaged governing equations with coarse grids will result in inaccurate flow prediction because the heterogeneous gas–solid flow structures are not captured in detail [7–9].

In addition to the inaccuracies caused by averaging, a key challenge in modeling fluidized bed flow is predicting the phase interaction (i.e., the drag

force). The local drag force inside the fluidized bed will dominate the solid flow and transport in the system. The conventional homogeneous drag models proposed by Ergun [10] and Wen and Yu [11] are widely used to describe the phase interaction in fluidized bed investigations. Note that these drag models were derived for a liquid–solid homogeneous suspension from bed expansion data (i.e., stationary solids). Drag models derived for homogeneous suspensions in heterogeneous systems will not predict the flow properties accurately. In macroscopic models, homogeneous drag models overpredict the drag force of heterogeneous flows, and the applied drag should be reduced. Matsen [12] made an early attempt to derive this drag correction in the macroscopic domain for gas–solid flows by deriving a drag correction for dilute gas–solid suspensions in an entrainment flow region. In this approach, a drag correction was introduced in the form of a dimensionless slip velocity with respect to the solid volume fraction. A solid volume fraction of $\alpha_s = 0.1$ was used to divide the drag correction into the dilute and dense regions. Sankar and Smith [13] extended Matsen's correction parameters to various materials, particle sizes, and riser diameters. Using a modified version of the correction parameters of Sankar and Smith, Hyppänen [14] applied the drag correction in a circulating fluidized bed (CFB) simulation

tool. Kallio [15] later derived a correlation for the macroscopic drag correction parameters of Matsen as a function of the Archimedes number. A similar type of macroscopic drag correction was applied by Shah et al. [16] in an industrial-scale CFB simulation using the Eulerian–Eulerian CFD approach. In these earlier works, the dilute flow region was defined as having a solid volume fraction of $\alpha_s < 0.1$, which originated from the work of Matsen for an entrainment flow region. It is questionable to use these drag correction parameters under CFB conditions, because they were intended to describe another flow region. There are also macroscopic correlations for drag force correction in the literature [17] that can be used for specific applications and in a limited operating range. Usually, these drag corrections are correlated with the local packing density and do not consider the system's total inventory. In addition to the macroscopic drag correction approaches, the filtered drag correction method of Igci et al. [18] and energy-minimization multi-scale (EMMS) drag correction method of Li et al. [19] and Li [20] have been used to investigate macroscopic heterogeneous gas–solid flows. Both of these well-known methods are used to model subgrid-scale flow structures assuming a heterogeneous system. In the filtered drag correction, local heterogeneity is obtained from a detailed numerical simulation, and coarse-

grained drag information is modeled at a larger scale. The obtained drag correction is applicable only to materials with spherical particles of uniform size. In the EMMS drag correction, the local heterogeneity and drag force are estimated using three homogeneous gas–solid subsystems: the cluster phase, dilute phase, and interphase; a material with spherical particles of uniform size is also assumed. Several model variants are available for the EMMS drag correction, and the details of the drag model, which significantly affect the final result, are mainly empirical or semi-empirical [1]. Hence, for different materials and application scales, there is no clear agreement on the type of drag correction or the parameters to be used in practical macroscopic investigations. For the gas–solid interaction, it is a great challenge to identify the connections between the real material properties, including the particle size, shape and density distributions, and the level of local heterogeneity. For example, irregular and smooth, round particles with the same size distribution lead to very different momentum interactions. However, it is necessary to investigate coupled and practical processes with sufficiently accurate transport properties of real materials. Consequently, practical methods of investigating complex processes under steady-state and transient conditions are needed.

In this study, a practical characterization method for gas–solid flows is

presented in which the gas–solid drag including local heterogeneity is defined. In this method, characteristic drag is determined for a real solid material having particle size, shape and density distributions. The result is obtained directly from the experiments and can thus be connected to the real representative material used in the experiments and e.g. compare with drag force correlations of equivalent size of smooth and round particles. Characterization based drag represents a more reliable, real estimate of momentum interaction compared to existing drag correlations. In addition, a 1D gas–solid flow simulation tool that is capable of transient simulations is presented. This simulation tool solves the simplified momentum equation for the solid phase to provide a realistic physical description of the transient flow behavior. The total momentum transfer obtained from the material flow characterization is applied to the simulation tool to compensate for the errors resulting from momentum equation simplifications and model discretization. The characterization method with drag correction for a real solid material and the 1D simulation tool are studied and validated within a frame of experimental results from laboratory-scale CFB equipment. The transient prediction capability of the simulator is tested using the step and ramp functions of the CFB system. The use of the results obtained through the characterization method

is limited to the test device and material associated with the characterization data. However, the characterization method presented is universally valid and scalable. Characterization reveals the magnitude of the momentum interaction associated with the material in question relative to other materials. A similar relative phase interaction and solid transport in the gas-solid flow are also expected on a large scale. The quantitative reliability of characterization in larger-scale predictions can be improved as the number of plant-scale validations increases. In order to compare the quantitative results, the presented method can be used to retrieve the magnitude of the drag force corresponding to the large-scale measurements. The presented characterization method can also be used directly to generate a simplified large-scale flow model for a given material if adequate plant measurements are available.

2. Numerical model

An Eulerian–Eulerian time-dependent 1D model was developed for a macroscopic gas–solid fluidized bed flow. This numerical model is used to determine the drag force correction parameters using the experimental results. After the function fitting procedure of the drag force correction parameters,

this model is used to validate the flow model and the drag force characterization method. In addition, the model is used in the implementation of flow simulation cases. The mass conservation equation was applied for the gas (g) and solid (s) phases, and the momentum conservation equation was applied for the solid phase. In this approach, gas velocity is solved using the mass balance. The momentum equations of the gas and solid phases have been used to calculate the pressure. The pressure calculation includes the effects of gravity and acceleration of both phases. The gas–wall and solid–wall interactions were neglected, and their effects were included in the drag force term. Solid–solid interaction was omitted as only one continuous solid phase was under consideration. The omission of wall effects and internal forces in the phases guarantees a simple and numerically efficient momentum equation. The sources of error resulting from the simplifications are included in the drag force correction based on the characterization method. The gas and solid material were assumed to have a constant density. The simplified governing equations are as follows:

Conservation of mass:

$$\frac{\partial \bar{\alpha}_g}{\partial t} + \frac{\partial \left(\bar{\alpha}_g \tilde{v}_g\right)}{\partial z} = 0 \tag{1}$$

$$\frac{\partial \bar{\alpha}_s}{\partial t} + \frac{\partial \left(\bar{\alpha}_s \tilde{v}_s\right)}{\partial z} = 0 \tag{2}$$

Conservation of momentum:

$$\rho_s \bar{\alpha}_s \frac{\partial \tilde{v}_s}{\partial t} + \rho_s \bar{\alpha}_s \tilde{v}_s \frac{\partial \tilde{v}_s}{\partial z} = -\bar{\alpha}_s \frac{\partial \bar{p}}{\partial z} - \rho_s \bar{\alpha}_s g + \bar{K}_{gs} \left(\tilde{v}_g - \tilde{v}_s\right) \tag{3}$$

Reynolds averaging was used for the packing fractions $\bar{\alpha}$, pressure $\bar{p}$, and drag exchange coefficient $\bar{K}_{gs}$. Favre averaging was used for the velocities $\tilde{v}$. Fully implicit time discretization and first-order upwind space discretization schemes were used to build the model frame. The implicit time iteration was controlled by relaxation factors with residual limits of 10^{-6}. The time step size was based on the Courant number, Co = 0.3, which was calculated for the maximum solid velocity in the system. In the space discretization, a uniform grid size and staggered grid were applied. The pressure gradient was defined using the gravitational and acceleration terms for both materials. The approach of Wen and Yu [11] was employed to define the drag exchange coefficient $\bar{K}_{gs}$ multiplied by a correction factor H_d. For a discretized 1D element i, the local drag correction $H_{d,i}$ is defined as

$$H_{d,i} = \alpha_{g,i}^{2.65} \left(\frac{v_{sl}}{v_t}\right)^{-2} \tag{4}$$

where the dimensionless slip velocity is by Matsen [12]

$$\frac{v_{sl}}{v_t} = A\alpha_{s,i}^{B} \tag{5}$$

Matsen [12] proposed this empirical correlation for dilute flows (i.e., $\alpha_{s,i} < 0.1$) on the basis of experimental data for entrainment phenomena with constant parameters $A = 10.8$ and $B = 0.293$. For dense flows (i.e., $\alpha_{s,i} > 0.1$), Matsen derived a correlation for the dimensionless slip velocity on the basis of the bubbling bed expansion according to two-phase flow theory. Sankar and Smith [13] experimentally studied the countercurrent downflow of solids in narrow vertical pipes and derived the correlations for the empirical parameters A and B as a function of the properties of the gas and solid material and of the pipe diameter. Kallio [15] later correlated the parameters A and B in the dilute region as a function of the Archimedes number using literature data. According to Wirth [21], the distribution of solids in the CFB riser is proportional to the superficial gas velocity together with the total solid inventory of the system. In the current study, the effect of gas velocity and solid inventory have been considered by correlating the parameters A and B with the gas superficial velocity U_g and the average solid fraction $\alpha_{s,av}$ in

the system. In addition, the dimensionless slip velocity according to Eq. 5 is considered in the entire range of the local solid fraction $\alpha_{s,i} > 0$.

The external solid circulation in the CFB loop was approximated by a simple time delay model to consider the dynamic behavior of the system. This model controlled the input solid flow $q_{m,s,in}$ into the riser bottom element with a target riser mass $m_{s,target}$ and time constant τ. The model of the input solid flow is expressed in Eq. 6

$$q_{m,s,in} = q_{m,s,exit} - \frac{m_{s,tot} - m_{s,target}}{\tau} \tag{6}$$

3. Results and discussion

3.1. Experimental results

Experiments were performed in a CFB cold unit operated in air at ambient temperature and pressure. Fig. 1 shows a schematic illustration of the CFB cold unit, which consists of a riser, cyclone, material weighing unit at the downcomer, and loop seal. The riser height is 1.88 m, and the inner diameter is 0.11 m. Mass flow controllers regulate the airflow to the riser and loop seal. Several pressure measurement probes are placed along the riser to obtain the material distribution inside the riser. The circulation of

solid material in the system was also measured. A pinch valve is mounted in the downcomer and is supported by three strain gauges. The circulation of solid material was measured by closing the pinch valve and measuring the accumulated mass in real time using the strain gauges. From the strain gauge data, the mass circulation rate was calculated as the time derivative of the mass accumulation. The measurements were repeated five times for each balance, and the average circulation rate was calculated.

$CaCO_3$ powder with a density of 2770 kg/m^3 and an average particle diameter of 237 μm was used in the experiments. The average particle size and particle size distribution (Fig. 2a) were determined by image analysis of material sample. Fig. 2b shows the distribution of the probable particle terminal velocity, which is calculated by using a method presented by Gidaspow [2], and the particle size distribution at the normal pressure and temperature (NTP) in air. Terminal velocity for each particle size fraction is obtained from the simple force balance of buoyancy due to gravity and drag force of single sphere. Correlations by Rowe [22] are used for single-particle drag coefficient. The particle terminal velocity for an average particle size of 237 μm is 1.63 m/s.

A total of 15 fluidization tests were performed at five superficial gas ve-

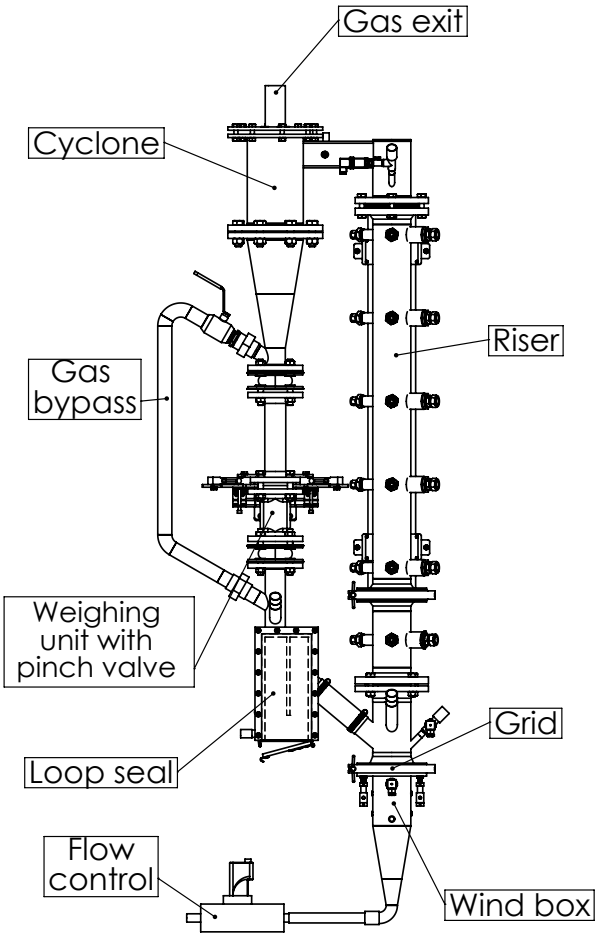

Figure 1: Schematic of CFB cold unit.

locities and three loop seal gas velocities. All of the superficial gas velocities were higher than the terminal velocity of particles of the average size. On the basis of the loop seal geometry and fluidized air feed system, half of the loop seal flow was assumed to travel to the riser. The air feeds and riser pressure values were recorded at 1 s intervals. The stabilized pressure values

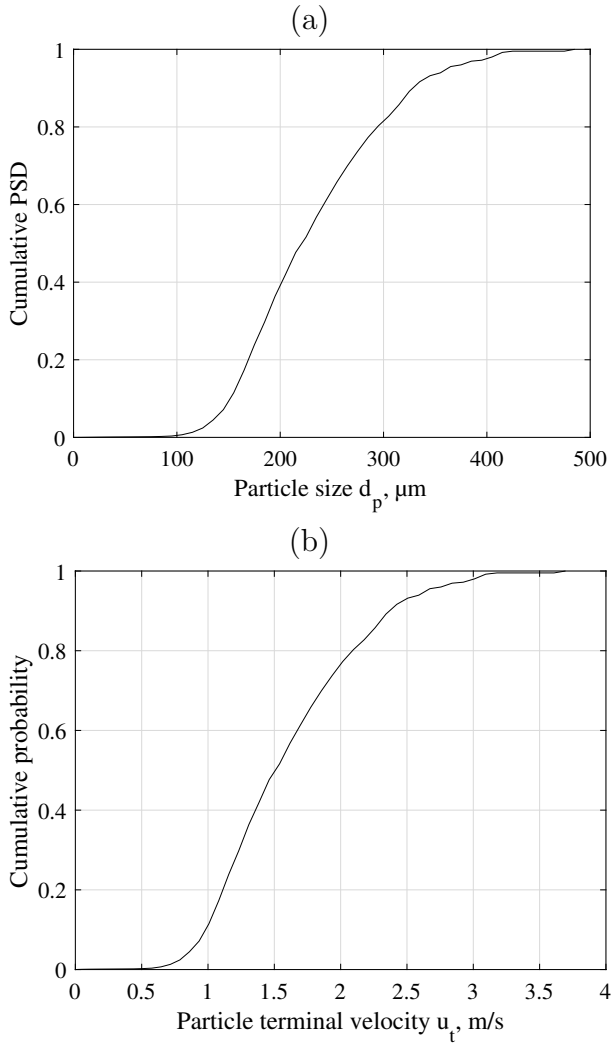

Figure 2: (a) Particle size distribution (PSD) and (b) particle terminal velocity distribution for the $CaCO_3$ used in the experiments.

were recorded between consecutive solid circulation measurements, and the average values were calculated in a post-processing step. The set values of

the air feeds and measured quantities are shown in Table 1.

Table 1: Set values of air feeds and measured quantities. Reference pressure set to zero at an elevation of 1.75 m from the grid.

Case	$U_{g,r}$	$U_{g,LS}$	$U_{g,av}$	$q_{m,s}$	p_6 (0.0 m)	p_5 (0.07 m)	p_4 (0.33 m)	p_3 (0.7 m)	p_2 (1.0 m)	p_1 (1.3 m)
No.	[m/s]	[m/s]	[m/s]	[g/s]	[Pa]	[Pa]	[Pa]	[Pa]	[Pa]	[Pa]
1	2.0	0.1	2.115	27.7	1454	736	144	93	59	32
2	2.0	0.2	2.117	31.5	1647	918	154	99	63	34
3	2.0	0.3	2.225	38.0	1718	987	178	114	72	39
4	2.5	0.1	2.586	54.9	1454	747	234	155	99	55
5	2.5	0.2	2.639	60.2	1603	884	253	166	106	59
6	2.5	0.3	2.696	72.5	1643	918	273	179	114	64
7	3.0	0.1	3.115	124.5	1098	662	375	261	173	101
8	3.0	0.2	3.175	141.4	1225	734	406	279	184	108
9	3.0	0.3	3.207	150.6	1273	765	420	288	190	112
10	3.5	0.1	3.591	120.4	981	507	317	232	163	101
11	3.5	0.2	3.637	163.7	1153	640	392	282	195	120
12	3.5	0.3	3.751	188.8	1217	680	417	299	207	128
13	4.0	0.1	4.103	111.2	1029	445	292	221	161	105
14	4.0	0.2	4.181	146.3	1090	486	315	238	173	112
15	4.0	0.3	4.245	152.4	1116	454	298	226	166	110

3.2. Numerical analysis of individual test cases

Each of the experimental test cases listed in Table 1 was analyzed by the numerical tool introduced in Section 2. The key properties and parameters of the simulations are shown in Table 2. The riser is divided into 100 vertical elements with an element height of approximately seven particle diameters. In each simulation case, an empty riser was used as the initial configuration. The system was gradually filled with solids using an estimated value of the

initial solid target mass $m_{s,target}$. The simulation was continued until the steady state was reached.

Table 2: Properties and parameters of the numerical simulations.

Particle size	d_p	237 μm
Solid density	ρ_s	2770 kg/m^3
Gas density	ρ_g	1.1959 kg/m^3
Gas viscosity	μ_g	$1.85 \cdot 10^{-5}$ Ns/m^2
Riser diameter	d_r	0.11 m
Riser height	h_{tot}	1.75 m
Number of 1D elements	n_{tot}	100
Solid input time constant	τ	3 s

The main objective of the numerical analysis was to determine the most suitable values of the drag correction parameters A and B in each test case. The drag correction given in Eq. 5 was used. Nested iteration loops for the parameters A and B and for the total system mass $m_{s,tot}$ were applied with a measured solid circulation rate. The relative pressure error according to Eq. 7 was minimized to obtain the parameters A and B, and the system target mass $m_{s,target}$ was varied to obtain the measured grid pressure p_6.

$$E_p = \sqrt{\sum_{p_i=1}^{6} \left(\frac{p_{i,sim} - p_{i,exp}}{p_{i,exp}} \right)^2} \tag{7}$$

The accelerations of the gas and solid phases were included in the defini-

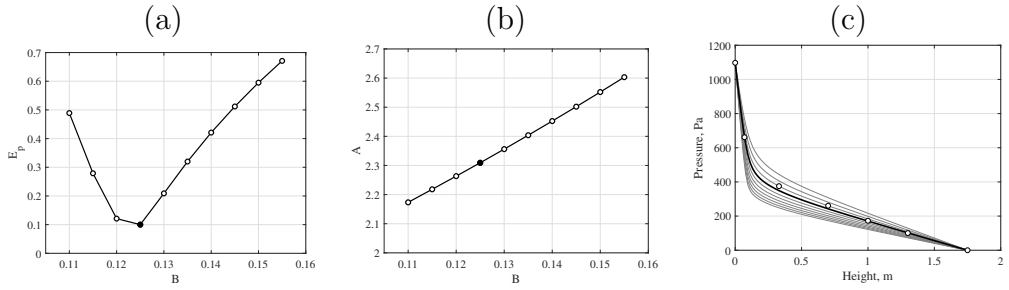

Figure 3: Iteration data for case 7. (a) Average pressure error E_p as a function of parameter B. (b) Parameter $A(B)$ dependency. (c) Simulated pressure profiles with corresponding parameters A and B. The filled symbols in (a) and (b) and black solid line in (c) represent the simulation data with the smallest relative pressure error. The open symbols in (c) show the measured pressure data, and the gray lines show all the simulated pressure profiles for case 7.

tion of the total pressure used in the iteration method for the solid mass in the system. In each iteration case, the solid circulation rate $q_{m,s}$ was obtained within an error of 0.1%.

Fig. 3 shows the iteration data for case 7. For all the test cases, similar iteration data were produced to provide the drag correction parameter B with the minimum pressure error E_p. In addition, the dependency between A and B was obtained.

3.3. Drag correction

A drag correction for real $CaCO_3$ powder with its particle size, shape and density distributions was developed on the basis of the numerical simulation data obtained from the individual test cases. The function forms for A and B were selected during numerical fitting by comparing the coefficient of determination of the different options. The steps of the drag correction

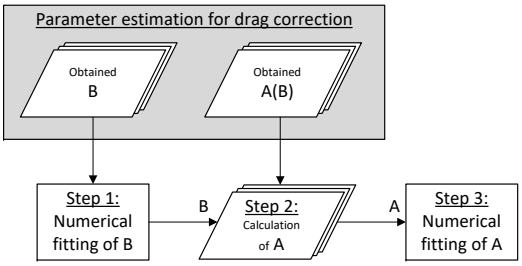

Figure 4: Flowchart for the development steps of drag correction.

development are shown in Fig. 4 and the corresponding steps are as follows:

Step 1:

The fitting function shown in Eq. 8 and numerical data from the individual test cases were used to obtain the values of the function parameters a_1, a_2, and a_3. The average solid fraction in the system, $\alpha_{s,av}$, was calculated using the total solid mass in the system in each test case.

$$B = a_1 + a_2 \left(U_g \alpha_{s,av}\right)^{a_3} \tag{8}$$

The values of B from each test case and the fitting function obtained using Eq. 8 are presented in Fig. 5. The parameter fitting procedure yielded numerical values of $a_1 = 0.0266$, $a_2 = 0.0657$, and $a_3 = -0.157$.

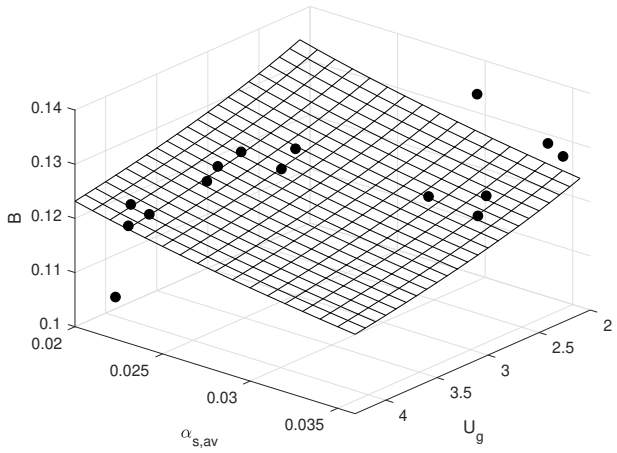

Figure 5: Numerical data obtained from individual test cases and fitting function of parameter B according to Eq. 8.

Step 2:

Iteration data from each test case were used to obtain the values of the drag correction parameter A. First, B was recalculated from the fitting function obtained in Step 1. The recalculated B was used to obtain the

corresponding A value from the iteration data. In this way, the circulation rate for the parameter pair A and B was maintained. Fig. 3b shows the dependency between the parameters A and B for case 7.

Step 3:

The fitting function shown in Eq. 9 and the numerical data for the parameter A were used to obtain the values of the function parameters a_i.

$$A = a_4 \exp\left(a_5 U_g + a_6 \alpha_{s,av}\right) U_g^{a_7} \alpha_{s,av}^{a_8} \tag{9}$$

Fig. 6 shows the values of A and the obtained fitting function according to Eq. 9. The parameter fitting procedure yielded numerical values of $a_4 = 0.0603$, $a_5 = 0.3372$, $a_6 = 23.15$, $a_7 = -0.5765$, and $a_8 = -0.7238$.

3.4. Validation of characterization method

The characterization method, including numerical model and drag correction, was validated by simulating the experimental cases shown in Table 1 using the proposed drag correction presented in Section 3.3. Validation using the experimental data included confirmation of selected drag correction function forms and parameters obtained by numerical fitting. In each validation case, the system target mass was varied to produce the measured

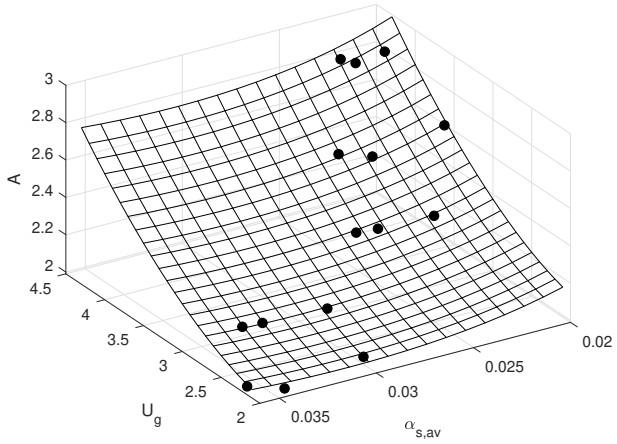

Figure 6: Numerical data obtained from individual test cases and fitting function for parameter A according to Eq. 9.

grid pressure p_6. In the validation simulations, the pressure profile and circulation rate were obtained using the simulation approach and drag correction. The validation data are shown in Fig. 7. The circulation rate and individual pressure values obtained in the validation simulations were reasonably accurate.

Validation cases 9 and 15 had the smallest and largest relative pressure errors E_p, respectively. The pressure data for these validation cases are shown in Fig. 8. The pressure data for case 9 are in excellent agreement with the measured values. Case 15 also shows good quantitative agreement with the experiments. For this case, only a small deviation is observed in the pressure

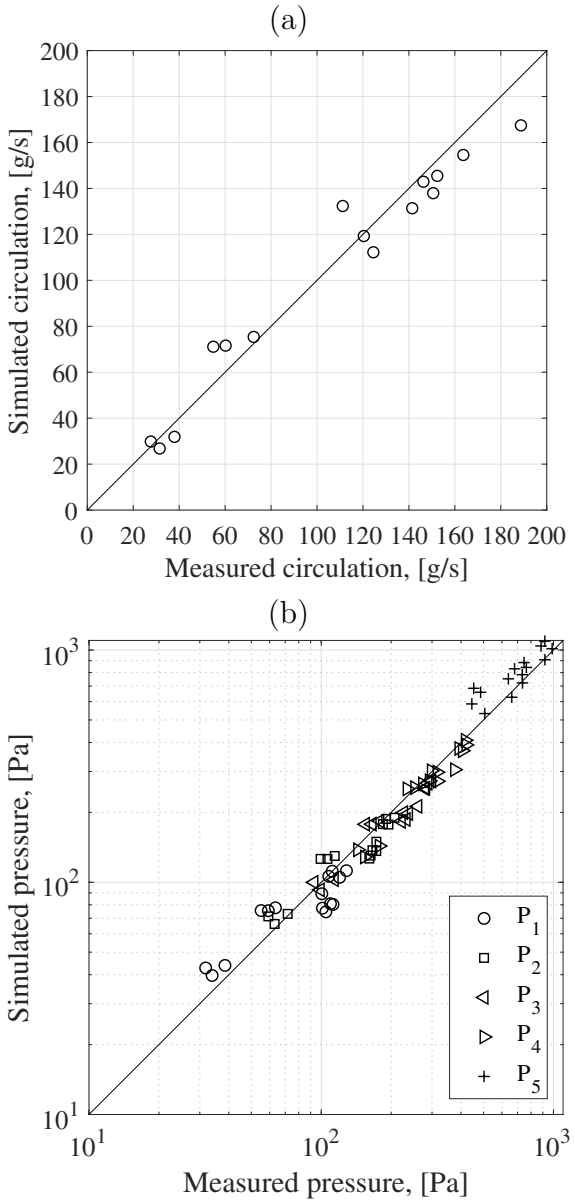

Figure 7: (a) Circulation rate and (b) pressure results of the validation simulations.

data for the bed region.

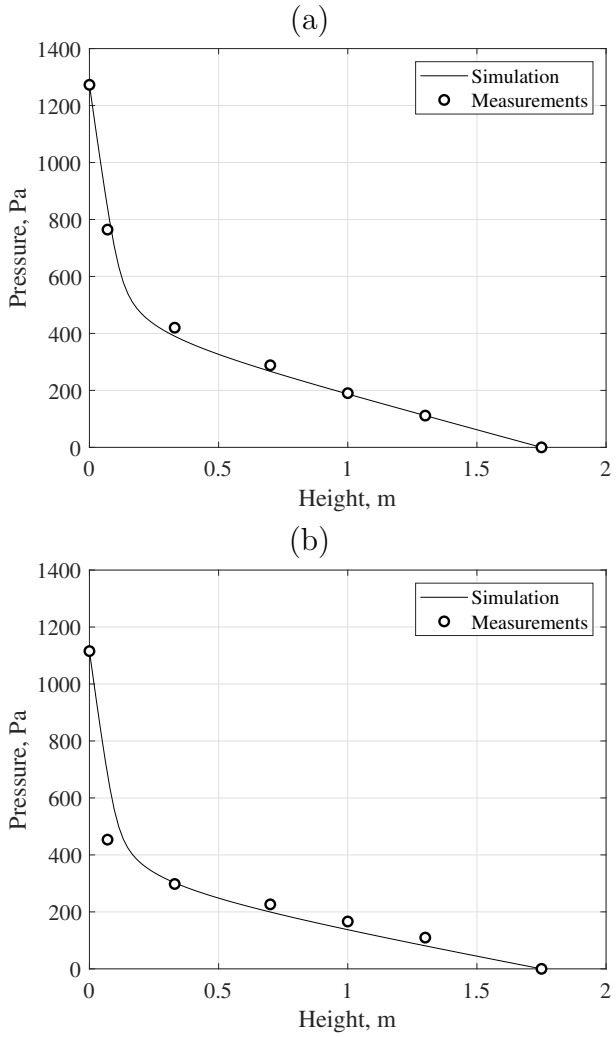

Figure 8: Simulated pressure profiles and measured pressures for the validation cases. (a) Case 9, which had the smallest pressure error, and (b) case 15, which had the largest pressure error.

The drag corrections for validation cases 1 and 15, which represent low and high gas velocities, are illustrated in Fig. 9. Both cases exhibit high drag reduction at higher local solid fractions. At the high gas velocity and lower total inventory, the maximum solid fraction at the riser bottom is lower than that obtained at the low gas velocity and higher total inventory. Macroscopic drag correction by Matsen [12] is presented as a basis for comparison. Compared drag models are designed for a different fluidization range and for different materials, and only quantitative comparison can be made. Characterization based drag correction predicts a lower correction at packing densities below 0.1 compared to drag correction by Matsen. At packing densities higher than 0.1, the function forms of the models are different and direct comparison is not possible. For drag correction models, there is a significant difference in operation, where the correction based on characterization changes according to fluidization velocity and solid inventory, whereas the correction according to Matsen uses constant function parameters. The applied drag correction and proposed 1D simulation tool quantitatively reproduced the expected behavior of the CFB riser in the studied range.

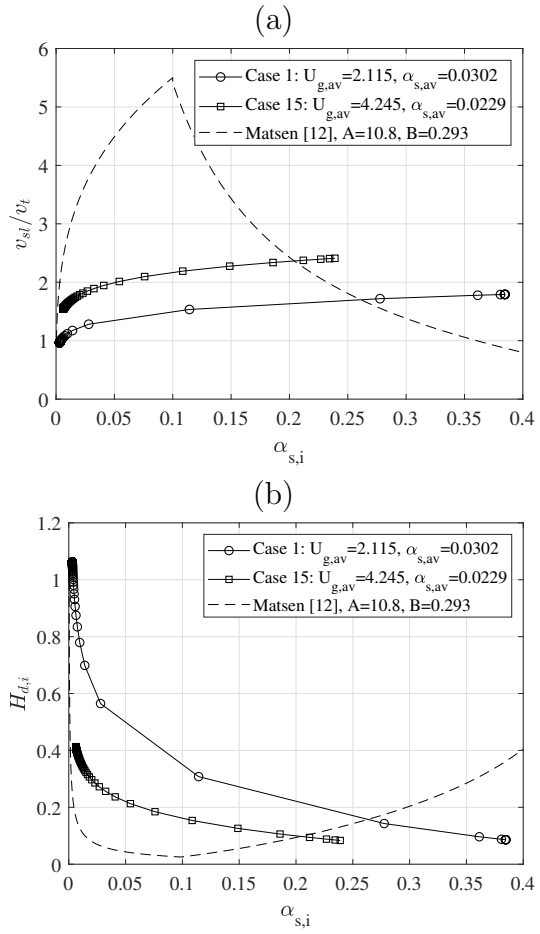

Figure 9: Drag corrections for validation cases 1 and 15, which are the low and high gas velocity cases, respectively. Results are shown as a function of the local solid fraction $\alpha_{s,i}$ of each 1D element. (a) Dimensionless slip velocity according to Eq. 5. (b) Drag approach of Wen and Yu corrected according to Eq. 4. Drag correction by Matsen [12] given for comparison.

3.5. Fluidization simulations

Fluidization simulations were conducted for different superficial gas velocities and mass inventories in the system. In these simulations, the operation of the CFB system outside of the validation range was also studied. Fig. 10 shows the boundary conditions and operation range of the simulations. A total of 25 simulations were conducted with five superficial velocities and five total solid masses in the system. The properties and parameters shown in Table 2 were used in each simulation, and the drag correction described in Section 3.3 was applied. An empty riser was used as the initial configuration in each simulation. The riser was filled by the inlet solid feed with a given target solid mass as a boundary condition. Each simulation was continued until the steady state was reached.

Figure 10: Illustration of fluidization simulation cases. Open symbols represent applied boundary conditions. Filled symbols represent boundary conditions obtained from experiments and used in the drag correction development and validation work.

Fig. 11 shows the simulation results for gas–solid fluidized bed operation in the given range. A low superficial gas velocity with low solid loading and a

high superficial gas velocity with higher loading are outside of the validation range. The simulation tool with drag correction applied can predict the fluidized bed operation with good accuracy near the validation points. The model is not designed for extrapolation and has some difficulty predicting the operation at a higher solid loading, which can be observed from the trends of the circulation rate and upper part of the solid fraction, as shown in Fig. 11a and c, respectively. In this extrapolated operation range, a higher solid fraction was expected in the upper part, and the circulation rate was expected to increase with increasing solid loading. The model predicted slight decreases in these quantities when the solid loading was increased beyond the validation range. Using experimental data for a wider operation range will provide additional knowledge of the flow behavior, which can support development of the drag correction.

(a) (b) (c)

Figure 11: Simulation results with drag correction. (a) Solid circulation rate, (b) bottom bed solid fraction, and (c) upper section solid fraction for various fluidization velocities and solid inventories.

The predicted fluidized bed operation is strongly affected by the pres-

ence and functional form of the drag correction. The drag correction in its current form defines the material distribution inside the riser according to the momentum balance. It also shows the net solid flow through the riser. To improve the ability of the model to forecast fluidized bed operation correctly in a wider range, the characterization and validation range should be extended.

4. Transient simulations

The use of fluidized bed reactors for a number of novel processes has been proposed because they provide good performance factors for multiphase reactions. Efficient and accurate tools are required for process design work and for the design of optimized process controls. The proposed 1D flow tool can perform transient, single reactor or coupled reactor flow simulations that provide a physical description using the momentum approach. This capability together with the mass balance ensures physically valid results for transient flow patterns and movement of solid mass and thermal energy during dynamic operation. Three simulations are performed as examples to illustrate the ability of the 1D model to predict transient operation of the CFB riser with the drag correction applied. The up step, down step,

and ramp functions of the gas superficial velocity are used in these transient simulations. Non-physical step changes have been used to demonstrate the model's ability to cope with a traditional numerical test case. For more realistic test cases, two ramp rates (R1: ± 0.05 m/s^2, R2: ± 0.025 m/s^2) are applied for the gas superficial velocity. Transient operation is investigated between two steady states, $U_g = 3.0$ m/s and $U_g = 3.5$ m/s, with an average solid fraction of $\alpha_{s,av} = 0.025$ in the riser. Fig. 12 shows the superficial gas velocity U_g in the riser in the transient simulations.

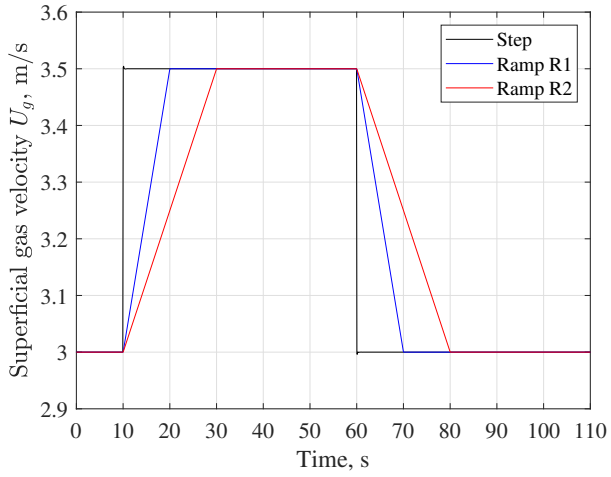

Figure 12: Superficial gas velocity U_g in the riser in the transient simulations. Ramp rates for U_g are R1 = ± 0.05 m/s^2 and R2 = ± 0.025 m/s^2

.

Fig. 13 shows the simulated solid packing fraction α_s profiles along the riser height h for the steady states at $U_g = 3.0$ m/s and $U_g = 3.5$ m/s.

Snapshots of the profiles are taken at $t = 5$ s and $t = 55$ s. At a higher superficial gas velocity, the solid packing fraction in the top section of the riser will be higher, and that in the bottom section will be lower.

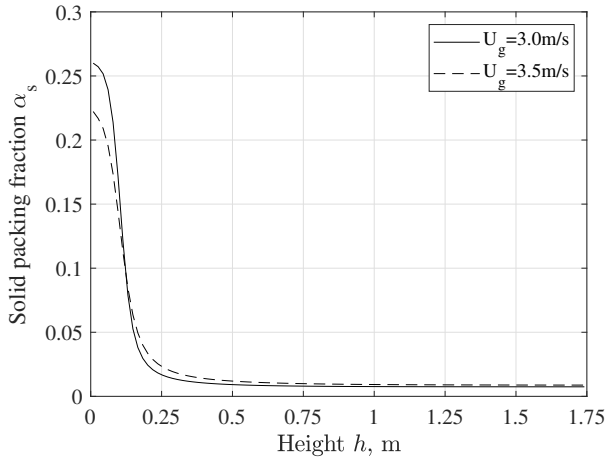

Figure 13: Simulated solid packing fraction profiles along the riser height under steady-state conditions.

The output solid mass flow rate and the local packing fractions at $h = 0.1$ m and $h = 1.6$ m during simulated transient operation of the CFB riser are shown in Figs. 14 and 15, respectively. A sudden transient step shows local fluctuations inside the riser. The numerical tool can predict operation under sudden changes, demonstrating its robustness and flexibility. In the ramp tests, the local flow parameters change smoothly as the ramp rate changes. A small time lag is observed in the response of the solid packing fraction in

the upper section of the riser. This time lag in the riser occurs because the momentum approach is used.

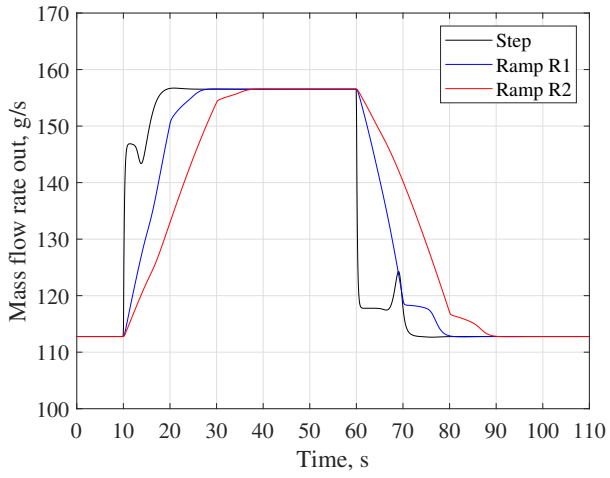

Figure 14: Solid mass flow rate from the riser with time. Transient operation is shown for step, ramp R1, and ramp R2 cases.

5. Conclusions

A method of characterizing the macroscopic gas–solid flow in a CFB and its validation within an experimental frame was introduced. This method enables predictions of the gas–solid flow based on the real properties of the solid material, including the real size, shape and density distributions, which affect the heterogeneity and gas–solid drag. Experimental data on the solid circulation rate and axial pressure profile were used to obtain a drag correc-

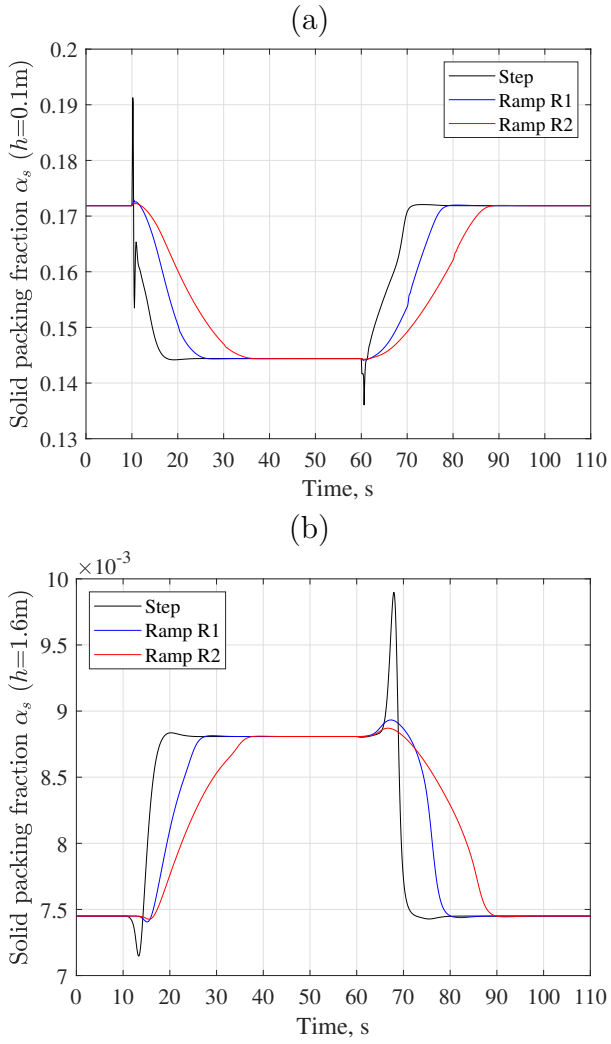

Figure 15: Solid packing fraction as a function of time for step operation and ramps R1 and R2. (a) Solid packing fraction at elevation of $h = 0.1$ m. (b) Solid packing fraction at elevation of $h = 1.6$ m.

tion for gas–solid flow. Drag corrections for individual test cases were used to derive a description of the drag correction function. When drag information from characterization tests based on the real material properties is used, the predictions of the gas–solid flow will be more realistic than those of previous drag models with simplified material properties. In the validation procedure, experimental balances were simulated with good accuracy using the proposed drag correction function. The range of the experimental data was limited to enable studies in a wider operational range with good accuracy. Extending the experimental case matrix would make it possible to improve the estimation accuracy for drag correction in the CFB riser. This improvement should include appropriate variation in the riser solid inventory and applied superficial velocity. In addition, online data for the solid circulation rate would make it possible to validate the model and characterization method under transient conditions. In this study, a characterization method and numerical tool for macroscopic gas–solid flow in a CFB were successfully demonstrated within a range of experimental data. It should be emphasized that the obtained drag correction function is directly applicable only to this CFB equipment and the solid material used here. However, the proposed characterization method and procedure can be utilized in many ways, e.g.

i) Time-dependent simulation method for stationary and transient flow investigation of real material more generally on the basis of experimental data delimited in a specific device ii) The momentum transfer of the real material can be characterized compared to other characterized materials iii) As with characterization methods in general, the material characterization method can also be applied to different conditions and devices at different size scales by combining the characterization result with limited experimental data between the devices. This characterization method will provide a simple and fast tool to investigate the CFB flow in existing equipment. Application of the proposed method at different size scales for the same material would make it possible to investigate the scaling effect on the drag resulting from the reactor dimensions and level of heterogeneity. Analyzes at different size scales would also make it possible to estimate the friction terms of the momentum equation, which were omitted in this study. This tool can be used to perform time-dependent studies in which the rate of change is defined by the solid momentum equation. These studies will provide a more realistic and physical description of transients than the use of a predefined time delay for the rate of change. This is essential in comprehensive process models that provide physical flow and material frame for other process phenomena,

e.g. such as the movement of solid heat capacities and their influence on energy balance. The improved accuracy of this approach is expected to support operation and control design of these gas–solid flow systems. This flow model approach can be applied to the process simulator, making it possible to investigate complex and coupled reactor systems with more accurate flow prediction including also dynamic performance of the system.

Acknowledgements

The authors acknowledge financial support for this research from the Academy of Finland under Grant No. 278641.

References

[1] J. Wang, Continuum theory for dense gas-solid flow: A state-of-the-art review, Chemical Engineering Science 215 (2020) 115428.

[2] D. Gidaspow, Multiphase Flow and Fluidization, Academic Press, San Diego, 1994.

[3] Y. Tsuji, T. Kawaguchi, T. Tanaka, Discrete particle simulation of two-dimensional fluidized bed, Powder Technology 77 (1993) 79 – 87.

[4] K. Chu, A. Yu, Numerical simulation of complex particle–fluid flows, Powder Technology 179 (2008) 104 – 114.

[5] N. Yang, W. Wang, W. Ge, J. Li, CFD simulation of concurrent-up gas–solid flow in circulating fluidized beds with structure-dependent drag coefficient, Chemical Engineering Journal 96 (2003) 71 – 80.

[6] S. Schneiderbauer, S. Puttinger, S. Pirker, P. Aguayo, V. Kanellopoulos, CFD modeling and simulation of industrial scale olefin polymerization fluidized bed reactors, Chemical Engineering Journal 264 (2015) 99 – 112.

[7] S. Sundaresan, Modeling the hydrodynamics of multiphase flow reactors: Current status and challenges, AIChE Journal 46 (2000) 1102–1105.

[8] J. Wang, M. van der Hoef, J. Kuipers, Why the two-fluid model fails to predict the bed expansion characteristics of Geldart A particles in gas-fluidized beds: A tentative answer, Chemical Engineering Science 64 (2009) 622 – 625.

[9] S. Benyahia, S. Sundaresan, Do we need sub-grid scale corrections for both continuum and discrete gas-particle flow models?, Powder Technol-

ogy 220 (2012) 2 – 6. Selected Papers from the 2010 NETL Multiphase Flow Workshop.

[10] S. Ergun, Fluid flow through packed columns, Chemical Engineering Progress 48 (1952) 89–94.

[11] C. Wen, Y. Yu, Mechanics of fluidization, Chemical Engineering Progress Symposium Series 62 (1966) 100 – 111.

[12] J. M. Matsen, Mechanisms of choking and entrainment, Powder Technology 32 (1982) 21 – 33.

[13] S. Sankar, T. Smith, Slip velocities in pneumatic transport part I, Powder Technology 47 (1986) 167 – 177.

[14] T. Hyppänen, An Experimental and Theoretical Study of Multiphase Flow in a Circulating Fluidized Bed, Ph.D. thesis, Lappeenranta University of Technology, 1989.

[15] S. Kallio, The role of the gas-solid drag force in CFB modelling of fluidization, Technical Report 2005-3, Åbo Akademi University, 2005.

[16] S. Shah, K. Myöhänen, S. Kallio, T. Hyppänen, CFD simulations of

gas–solid flow in an industrial-scale circulating fluidized bed furnace using subgrid-scale drag models, Particuology 18 (2015) 66 – 75.

[17] T. O'Brien, M. Syamlal, Particle cluster effects in the numerical simulation of a circulating fluidized bed, in: proceeding of the 4th International Conference on Circulating Fluidized Beds (1993), pp. 345 – 350.

[18] Y. Igci, A. Andrews IV, S. Sundaresan, S. Pannala, T. O'Brien, Filtered two-fluid models for fluidized gas-particle suspensions, AIChE Journal 54 (2008) 1431–1448.

[19] J. Li, Y. Tung, M. Kwauk, Method of energy minimization in multi-scale modeling of particle-fluid two-phase flow, in: P. Basu, J. F. Large (Eds.), Circulating Fluidized Bed Technology, Pergamon, 1988, pp. 89 – 103.

[20] J. Li, Particle-fluid two-phase flow: The energy-minimization multi-scale method, Metallurgical Industry Press, 1994.

[21] K.-E. Wirth, Axial pressure profile in circulating fluidized beds, Chemical Engineering & Technology 11 (1988) 11–17.

[22] P. Rowe, Drag forces in a hydraulic model of a fluidized bed, Part II, Transactions of the Institution of Chemical Engineers 39 (1961) 175–180.